Interelectronic-interaction effects on the two-photon decay rates of heavy He-like ions

A. V. Volotka,[1,2,3,4] A. Surzhykov,[1,2] V. M. Shabaev,[4] and G. Plunien[3]
[1]*Physikalisches Institut, Universität Heidelberg, D-69120 Heidelberg, Germany*
[2]*GSI Helmholtzzentrum für Schwerionenforschung, D-64291 Darmstadt, Germany*
[3]*Institut für Theoretische Physik, Technische Universität Dresden, Mommsenstrasse 13, D-01062 Dresden, Germany*
[4]*Department of Physics, St. Petersburg State University, Oulianovskaya 1, Petrodvorets, 198504 St. Petersburg, Russia*
(Received 11 March 2011; published 14 June 2011)

Based on a rigorous quantum electrodynamics (QED) approach, a theoretical analysis is performed for the two-photon transitions in heavy He-like ions. Special attention is paid to the interelectronic-interaction corrections to the decay rates that are taken into account within the two-time Green-function method. Detailed calculations are carried out for the two-photon transitions $2\,^1S_0 \to 1\,^1S_0$ and $2\,^3S_1 \to 1\,^1S_0$ in He-like ions within the range of nuclear numbers $Z = 28$–92. The total decay rates together with the spectral distributions are given. The obtained results are compared with experimental values and previous calculations.

DOI: 10.1103/PhysRevA.83.062508 PACS number(s): 31.30.J−, 31.15.ac, 32.70.Cs

I. INTRODUCTION

The two-photon process involving simultaneous emission of two photons was theoretically predicted by Göppert-Mayer in 1931 [1]. It arises from a second-order interaction between an atom and the electromagnetic field, resulting in a sharing of the transition energy between the two photons. The energy distribution of the two-photon spontaneous emission forms a continuous spectrum in contrast to the one-photon process, where the photon frequency is equal to the transition energy. Various characteristics of the two-photon transitions, such as total and energy-differential decay rates, and angular and polarization correlations of the emitted photons, were widely investigated for heavy hydrogenlike ions (see, e.g., Refs. [2–6]). Due to recent advances in the experimental technique, heavy He-like ions have become promising candidates for studying two-photon decays in the high-Z domain. Here the $2\,^1S_0$ state is of special interest, since this state decays primarily into the ground state via two-photon emission. The first theoretical two-photon decay rate of the $2\,^1S_0$ state in helium was presented by Dalgarno [7]. Later, accurate nonrelativistic calculations, including the estimation of the relativistic effects, of the two-photon transition rates $2\,^1S_0 \to 1\,^1S_0 + 2\gamma(\mathrm{E1})$ for He-like ions were performed by Drake [2]. The two-photon decay $2\,^3S_1 \to 1\,^1S_0 + 2\gamma(\mathrm{E1})$ was investigated theoretically as well [8,9], although its rates are smaller than the corresponding one-photon M1 rates by a factor of about 10^{-4}. Up to now, the most accurate fully relativistic calculations of the two-photon decay rates of the $2\,^1S_0$ and $2\,^3S_1$ states in the highly charged ions were performed using relativistic configuration-interaction wave functions in Ref. [10]. Apart from the total and energy-differential decay rates, the angular correlations in the two-photon decay of He-like ions have also been investigated recently [11].

The lifetimes of the metastable $2\,^1S_0$ level in He-like ions have been measured up to $Z = 41$. The most precise measurements have been made in Kr^{34+} [12], Br^{33+} [13], and Ni^{26+} [14], where uncertainties of about 1% have been reported. However, up to now the two-photon decay of the $2\,^3S_1$ level in He-like ions has not been observed. As opposed to the total decay rate measurements, the observation of the energy-differential spectrum carries more detailed information about the entire atomic structure. Several experimental efforts have been made during the past two decades to accurately determine the spectral shape of the two-photon distribution for $2\,^1S_0$ decay in He-like ions [15–17]. The cleanest spectrum has been obtained recently in Refs. [18,19], unambiguously confirming predictions of relativistic many-body theory as compared to the nonrelativistic calculations.

Since the two electrons in He-like ions are strongly correlated, it is important to take into account the interelectronic-interaction effects when studying two-photon decays. In previous calculations, the correlation effects were accounted for by means of nonrelativistic Hylleraas variational wave functions [2], relativistic configuration-interaction (CI) wave functions [10], or by means of relativistic wave functions in screening potentials [11,19–21]. However, a rigorous description of high-Z systems requires the quantum electrodynamic (QED) approach, which treats systematically radiative and correlation corrections order by order. Future progress in the experimental techniques will allow us to observe QED corrections to the transition amplitudes. In particular, recent precise measurements of the one-photon decay rates of the $(1s^2 2s^2 2p)\,^2P_{3/2}$ state in B-like Ar [22,23] have been shown to be sensitive to the one- and many-electron QED effects [24–26]. The QED treatment of the correlation effects differs from the many-body perturbation theory by the frequency-dependent contribution. The first QED evaluation of the interelectronic-interaction correction of first order in $1/Z$ to the one-photon decay rates was performed in Ref. [27] employing the two-time Green-function method [28–30]; later these calculations were confirmed in Ref. [31] by means of the line profile approach [32]. The main goals of the present paper are the derivation of formulas for the interelectronic-interaction corrections to the two-photon decays from the first principles of QED and the numerical evaluations of the two-photon transitions $2\,^1S_0 \to 1\,^1S_0$ and $2\,^3S_1 \to 1\,^1S_0$ in the He-like ions. The paper is organized as follows: In the next section, the process of the two-photon emission is described in the framework of the two-time Green-function method. The calculation formulas for the first-order interelectronic-interaction corrections to the two-photon transition amplitude

are derived starting in the zeroth-order approximation with the Coulomb potential of the nucleus and with a local screening potential. In Sec. III, we present the numerical results for the two-photon decay rates of $2\,^1S_0$ and $2\,^3S_1$ states in He-like ions. Beyond the dominant channel of the emission of two electric-dipole (E1) photons, the higher multipoles contributions are also taken into account. The total and energy-differential decay rates are presented within the range of nuclear numbers $Z = 28 - 92$. Comparison with previous theoretical calculations and with experiment are given. We close with a short summary, in which we point out the main achievements of the present work.

Relativistic units ($\hbar = 1, c = 1, m = 1$) and the Heaviside charge unit [$\alpha = e^2/(4\pi)$, $e < 0$] are used throughout the paper.

II. BASIC FORMULAS

According to the basic principles of QED [33], the transition probability from the electronic state A to B accompanied by the emission of two photons with wave vectors k_{f_1}, k_{f_2} and polarizations ϵ_{f_1}, ϵ_{f_2}, respectively, is given by

$$dW_{B;A}(k_{f_1},\epsilon_{f_1},k_{f_2},\epsilon_{f_2}) = 2\pi\left|\tau_{\gamma_{f_1},\gamma_{f_2},B;A}\right|^2\delta\left(E_B + k^0_{f_1} + k^0_{f_2} - E_A\right)d\mathbf{k}_{f_1}d\mathbf{k}_{f_2}, \quad (1)$$

where $\tau_{\gamma_{f_1},\gamma_{f_2},B;A}$ is the transition amplitude, which is related to the S-matrix element by

$$S_{\gamma_{f_1},\gamma_{f_2},B;A} = \left\langle k_{f_1},\epsilon_{f_1},k_{f_2},\epsilon_{f_2};B\left|\hat{S}\right|A\right\rangle = 2\pi i\,\tau_{\gamma_{f_1},\gamma_{f_2},B;A}\,\delta\left(E_B + k^0_{f_1} + k^0_{f_2} - E_A\right), \quad (2)$$

where E_A and E_B are the energies of the initial state A and the final state B, respectively. According to the standard reduction technique, the S-matrix element can be written as

$$S_{\gamma_{f_1},\gamma_{f_2},B;A} = -Z_3^{-1}\int d^4y_1 d^4y_2 \frac{\epsilon^{\nu_1 *}_{f_1}\, e^{ik^\mu_{f_1}y_{1\mu}}}{\sqrt{2k^0_{f_1}(2\pi)^3}}\frac{\epsilon^{\nu_2 *}_{f_2}\, e^{ik^\mu_{f_2}y_{2\mu}}}{\sqrt{2k^0_{f_2}(2\pi)^3}} \times\langle B|T j_{\nu_1}(y_1) j_{\nu_2}(y_2)|A\rangle\,, \quad (3)$$

where $j_\nu(y) = (e/2)[\overline{\psi}(y)\gamma_\nu,\psi(y)]$ is the Dirac current density operator and Z_3 is a renormalization constant for the emitted photon lines [34]. Here the electron-positron current operator $j_\nu(y)$ as well as the initial and final state vectors are given in the Heisenberg picture. Equation (3) can be written as

$$\begin{aligned} S_{\gamma_{f_1},\gamma_{f_2},B;A} &= -2\pi Z_3^{-1}\delta\left(E_B + k^0_{f_1} + k^0_{f_2} - E_A\right)\int d\mathbf{y}_1 d\mathbf{y}_2 A^{\nu_1 *}_{f_1}(\mathbf{y}_1)A^{\nu_2 *}_{f_2}(\mathbf{y}_2)\int_{-\infty}^{\infty} dt\, e^{ik^0_{f_1}t}\,\langle B|T j_{\nu_1}(t,\mathbf{y}_1)j_{\nu_2}(0,\mathbf{y}_2)|A\rangle \\ &= -2\pi Z_3^{-1}\delta\left(E_B + k^0_{f_1} + k^0_{f_2} - E_A\right)\int d\mathbf{y}_1 d\mathbf{y}_2 A^{\nu_1 *}_{f_1}(\mathbf{y}_1)A^{\nu_2 *}_{f_2}(\mathbf{y}_2)\left[\int_0^{\infty} dt\, e^{ik^0_{f_1}t}\,\langle B|j_{\nu_1}(t,\mathbf{y}_1)j_{\nu_2}(0,\mathbf{y}_2)|A\rangle\right. \\ &\quad \left. + \int_{-\infty}^{0} dt\, e^{ik^0_{f_1}t}\,\langle B|j_{\nu_2}(0,\mathbf{y}_2)j_{\nu_1}(t,\mathbf{y}_1)|A\rangle\right], \end{aligned} \quad (4)$$

where

$$A^\nu_f(\mathbf{x}) = \frac{\epsilon^\nu_f\, e^{i\mathbf{k}_f\cdot\mathbf{x}}}{\sqrt{2k^0_f(2\pi)^3}} \quad (5)$$

is the wave function of the emitted photon.

To evaluate this S-matrix element, the information about the entire atomic structure is needed. This information is contained in the Green functions. To obtain this information and to formulate perturbation theory, we employ the two-time Green-function method [28–30]. We introduce the following Green function to describe the process of a two-photon emission by an N-electron ion

$$\begin{aligned} &\mathcal{G}_{\gamma_{f_1},\gamma_{f_2}}\left(E',E,k^0_{f_1};\mathbf{x}'_1,\ldots,\mathbf{x}'_N;\mathbf{x}_1,\ldots,\mathbf{x}_N\right)\delta\left(E' + k^0_{f_1} + k^0_{f_2} - E\right) \\ &= \left(\frac{i}{2\pi}\right)^2\frac{1}{N!}\int_{-\infty}^{\infty} dx^0 dx'^0\int d^4y_1 d^4y_2\, e^{iE'x'^0 - iEx^0 + ik^0_{f_1}y^0_1 + ik^0_{f_2}y^0_2}\, A^{\nu_1 *}_{f_1}(\mathbf{y}_1)A^{\nu_2 *}_{f_2}(\mathbf{y}_2) \\ &\quad\times\langle 0|T\psi(x'^0,\mathbf{x}'_1)\cdots\psi(x'^0,\mathbf{x}'_N)j_{\nu_1}(y_1)j_{\nu_2}(y_2)\overline{\psi}(x^0,\mathbf{x}_N)\cdots\overline{\psi}(x^0,\mathbf{x}_1)|0\rangle\,, \end{aligned} \quad (6)$$

where $\psi(x)$ is the electron-positron field operator in the Heisenberg representation. In a general case, we imply that to zeroth approximation the vector A belongs to the s_A-dimensional subspace Ω_A of degenerate (or quasidegenerate) states, and the state B belongs to the s_B-dimensional subspace Ω_B. $P^{(0)}_A$ and $P^{(0)}_B$ are the projectors onto the corresponding subspaces,

$$P^{(0)}_A = \sum_{k_A=1}^{s_A} u_{k_A}u^\dagger_{k_A}\,, \quad P^{(0)}_B = \sum_{k_B=1}^{s_B} u_{k_B}u^\dagger_{k_B}\,, \quad (7)$$

and u_{k_A} and u_{k_B} are the unperturbed states of the N-electron system, constructed as linear combinations of one-determinant wave functions. From the spectral representation, we find that the Green function $\mathcal{G}_{\gamma_{f_1},\gamma_{f_2}}(E',E,k^0_{f_1})$ has isolated poles in the complex planes E' and E, at $E' \sim E^{(0)}_B$ and $E \sim E^{(0)}_A$, in the exact energies $E' = E_{k_B}$ and $E' = E_{k_A}$, respectively,

$$\begin{aligned}
&\mathcal{G}_{\gamma_{f_1},\gamma_{f_2}}\big(E',E,k^0_{f_1};\mathbf{x}'_1,\ldots,\mathbf{x}'_N;\mathbf{x}_1,\ldots,\mathbf{x}_N\big)\delta\big(E'+k^0_{f_1}+k^0_{f_2}-E\big)\\
&\quad=\frac{1}{2\pi}\frac{1}{N!}\sum_{k_A=1}^{s_A}\sum_{k_B=1}^{s_B}\frac{1}{E'-E_{k_B}}\frac{1}{E-E_{k_A}}\int d\mathbf{y}_1 d\mathbf{y}_2 A^{\nu_1 *}_{f_1}(\mathbf{y}_1)A^{\nu_2 *}_{f_2}(\mathbf{y}_2)\langle 0|\psi(0,\mathbf{x}'_1)\cdots\psi(0,\mathbf{x}'_N)|k_B\rangle\\
&\quad\times\left[\int_0^\infty dt\, e^{iE't-iE_{k_B}t+ik^0_{f_1}t}\,\langle k_B|j_{\nu_1}(t,\mathbf{y}_1)j_{\nu_2}(0,\mathbf{y}_2)|k_A\rangle+\int_{-\infty}^0 dt\, e^{iE_{k_A}t-iEt+ik^0_{f_1}t}\,\langle k_B|j_{\nu_2}(0,\mathbf{y}_2)j_{\nu_1}(t,\mathbf{y}_1)|k_A\rangle\right]\\
&\quad\times\langle k_A|\overline{\psi}(0,\mathbf{x}_N)\cdots\overline{\psi}(0,\mathbf{x}_1)|0\rangle+\text{terms regular at } E'\sim E^{(0)}_B \text{ or } E\sim E^{(0)}_A\,,
\end{aligned}\tag{8}$$

where $|k_A\rangle$ and $|k_B\rangle$ denote the states corresponding to the exact energies E_{k_A} and E_{k_B} from the subspaces Ω_A and Ω_B, respectively. Let us now project this Green function on the subspace of initial (Ω_A) and final (Ω_B) states,

$$g_{\gamma_{f_1},\gamma_{f_2},B;A}\big(E',E,k^0_{f_1}\big)=P^{(0)}_B\mathcal{G}_{\gamma_{f_1},\gamma_{f_2}}\big(E',E,k^0_{f_1}\big)\gamma^0_1\cdots\gamma^0_N P^{(0)}_A.\tag{9}$$

Comparing Eq. (4) with Eq. (8) and taking into account the definition (9), we obtain

$$\begin{aligned}
S_{\gamma_{f_1},\gamma_{f_2},B;A}&=Z_3^{-1}\delta\big(E_B+k^0_{f_1}+k^0_{f_2}-E_A\big)\oint_{\Gamma_B}dE'\\
&\quad\times\oint_{\Gamma_A}dE\; v^\dagger_B\, g_{\gamma_{f_1},\gamma_{f_2},B;A}\big(E',E,k^0_{f_1}\big)\,v_A\,,
\end{aligned}\tag{10}$$

where v_A and v_B are solutions of a generalized eigenvalue problem in the degenerate subspaces of the initial and final states, respectively (see Ref. [30] for details), the contours Γ_A and Γ_B enclose the poles corresponding to the initial and final levels, respectively, and exclude all other singularities of Green function $g_{\gamma_{f_1},\gamma_{f_2},B;A}$. Equation (10) represents the general relation between the S-matrix element of the two-photon transition and the two-time Green functions.

Afterwards, we consider the single initial and final states. In this case, the vectors v_A and v_B simply appear as normalization factors and the S-matrix element can be written as

$$\begin{aligned}
S_{\gamma_{f_1},\gamma_{f_2},B;A}&=Z_3^{-1}\delta\big(E_B+k^0_{f_1}+k^0_{f_2}-E_A\big)\\
&\quad\times\oint_{\Gamma_B}dE'\oint_{\Gamma_A}dE\; g_{\gamma_{f_1},\gamma_{f_2},B;A}\big(E',E,k^0_{f_1}\big)\\
&\quad\times\left[\frac{1}{2\pi i}\oint_{\Gamma_B}dE\; g_{BB}(E)\right]^{-1/2}\\
&\quad\times\left[\frac{1}{2\pi i}\oint_{\Gamma_A}dE\; g_{AA}(E)\right]^{-1/2},
\end{aligned}\tag{11}$$

where the Green functions g_{AA} and g_{BB} are defined by

$$\begin{aligned}
g_{AA}(E)&=\langle u_A|\mathcal{G}(E)\gamma^0_1\cdots\gamma^0_N|u_A\rangle\,,\\
g_{BB}(E)&=\langle u_B|\mathcal{G}(E)\gamma^0_1\cdots\gamma^0_N|u_B\rangle\,,
\end{aligned}\tag{12}$$

with

$$\begin{aligned}
&\mathcal{G}(E;\mathbf{x}'_1,\ldots,\mathbf{x}'_N;\mathbf{x}_1,\ldots,\mathbf{x}_N)\delta(E-E')\\
&\quad=\frac{1}{2\pi i}\frac{1}{N!}\int_{-\infty}^{\infty}dx^0dx'^0\,e^{iE'x'^0-iEx^0}\langle 0|T\,\psi(x'^0,\mathbf{x}'_1)\cdots\\
&\quad\times\psi(x'^0,\mathbf{x}'_N)\overline{\psi}(x^0,\mathbf{x}_N)\cdots\overline{\psi}(x^0,\mathbf{x}_1)|0\rangle\,.
\end{aligned}\tag{13}$$

The Green function $\mathcal{G}(E)$ contains the complete information about the energy levels of the ion [30]. The S-matrix element $S_{\gamma_{f_1},\gamma_{f_2},B;A}$ expressed in terms of the two-time Green functions $g_{\gamma_{f_1},\gamma_{f_2},B;A}$, g_{AA}, and g_{BB} via Eq. (11) can be calculated order by order by applying perturbation theory to the Green functions. The Feynman rules for the Green functions are given in Ref. [30].

In the following, we consider the two-photon transitions in He-like ions. The zeroth-order two-electron wave functions are constructed in the jj-coupling scheme as linear combinations

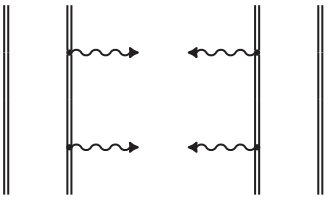

FIG. 1. The two-photon emission diagrams in the zeroth-order approximation. The double line indicates the electron propagators in the Coulomb field of the nucleus, while the photon emission is depicted by the wavy lines with arrows.

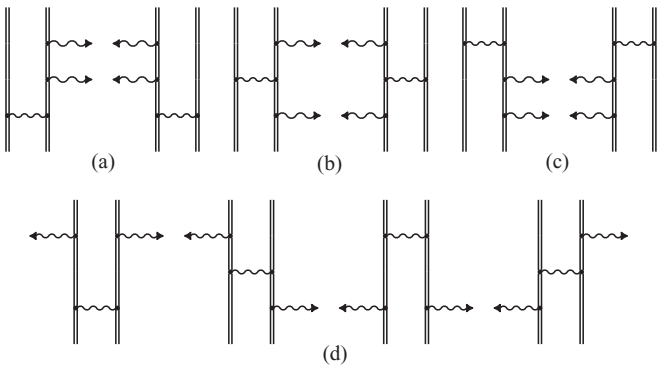

FIG. 2. Feynman diagrams representing the first-order interelectronic-interaction corrections to the two-photon emission. Notations are the same as in Fig. 1.

of the Slater determinants, $A = (a_1,a_2)_{J_A M_A}$, $B = (b_1,b_2)_{J_B M_B}$, as

$$u_A = F_A \frac{1}{\sqrt{2}} \sum_P (-1)^P |Pa_1 Pa_2\rangle\,, \tag{14}$$

where F_A denotes the shorthand notation for the summation over the Clebsch-Gordan coefficients

$$F_A|a_1a_2\rangle = \sum_{m_{a_1},m_{a_2}} C^{J_A M_A}_{j_{a_1} m_{a_1} j_{a_2} m_{a_2}} |a_1a_2\rangle \begin{cases} 1\,, & a_1 \neq a_2 \\ 1/\sqrt{2}\,, & a_1 = a_2, \end{cases} \tag{15}$$

J_A and j_a are the total angular momenta of the two- and one-electron wave functions, respectively, M_A and m_a are its corresponding projections, and P is the permutation operator, giving rise to the sign $(-1)^P$ of the permutation. The same notations hold for the final state B. The one-electron wave functions are found by solving the Dirac equation either with the Coulomb potential of the nucleus or with a local effective potential, which partly takes into account the interelectronic-interaction effects.

Furthermore, we consider the pure (nonresonant) two-photon decays. However, the question about cascades is beyond the scope of the present paper. This question was discussed in details in Ref. [35] and references therein. In the following, we also assume that the states A and B have at least one common one-electron state.

A. Zeroth-order approximation

To calculate the S-matrix element of the two-photon transition according to Eq. (11), we expand the two-time Green functions in perturbation series and combine the terms of the same order. The zeroth-order two-photon transition amplitude represented by diagrams in Fig. 1 is given by

$$S^{(0)}_{\gamma_{f_1},\gamma_{f_2},B;A} = \delta\big(E_B + k^0_{f_1} + k^0_{f_2} - E_A\big) \oint_{\Gamma_B} dE' \oint_{\Gamma_A} dE\, g^{(0)}_{\gamma_{f_1},\gamma_{f_2},B;A}\big(E',E,k^0_{f_1}\big)\,, \tag{16}$$

where the superscript "(0)" indicates the order of the perturbation theory. According to the Feynman rules, we obtain

$$\begin{aligned}
&g^{(0)}_{\gamma_{f_1},\gamma_{f_2},B;A}\big(E',E,k^0_{f_1}\big)\delta\big(E' + k^0_{f_1} + k^0_{f_2} - E\big) \\
&= F_A F_B \sum_P (-1)^P \int_{-\infty}^{\infty} dp^0_1 dp^0_2 dp'^0_1 dp'^0_2 dq^0\, \delta\big(E - p^0_1 - p^0_2\big)\, \delta\big(E' - p'^0_1 - p'^0_2\big) \\
&\times \Bigg\{ \langle Pb_2| \frac{i}{2\pi} \sum_{n_1} \frac{|n_1\rangle\langle n_1|}{p'^0_2 - u\varepsilon_{n_1}} \frac{2\pi}{i} R_{f_1} \delta\big(p'^0_2 + k^0_{f_1} - q^0\big) \frac{i}{2\pi} \sum_{n_2} \frac{|n_2\rangle\langle n_2|}{q^0 - u\varepsilon_{n_2}} \frac{2\pi}{i} R_{f_2} \delta\big(q^0 + k^0_{f_2} - p^0_2\big) \\
&\times \frac{i}{2\pi} \sum_{n_3} \frac{|n_3\rangle\langle n_3|}{p^0_2 - u\varepsilon_{n_3}} |a_2\rangle \langle Pb_1| \frac{i}{2\pi} \sum_{n_4} \frac{|n_4\rangle\langle n_4|}{p^0_1 - u\varepsilon_{n_4}} |a_1\rangle \delta\big(p'^0_1 - p^0_1\big) \\
&+ \langle Pb_1| \frac{i}{2\pi} \sum_{n_1} \frac{|n_1\rangle\langle n_1|}{p'^0_1 - u\varepsilon_{n_1}} \frac{2\pi}{i} R_{f_1} \delta\big(p'^0_1 + k^0_{f_1} - q^0\big) \frac{i}{2\pi} \sum_{n_2} \frac{|n_2\rangle\langle n_2|}{q^0 - u\varepsilon_{n_2}} \frac{2\pi}{i} R_{f_2} \delta\big(q^0 + k^0_{f_2} - p^0_1\big) \\
&\times \frac{i}{2\pi} \sum_{n_3} \frac{|n_3\rangle\langle n_3|}{p^0_1 - u\varepsilon_{n_3}} |a_1\rangle \langle Pb_2| \frac{i}{2\pi} \sum_{n_4} \frac{|n_4\rangle\langle n_4|}{p^0_2 - u\varepsilon_{n_4}} |a_2\rangle \delta\big(p'^0_2 - p^0_2\big) + (f_1 \leftrightarrow f_2) \Bigg\} \\
&= \frac{i}{2\pi} \frac{\delta\big(E' + k^0_{f_1} + k^0_{f_2} - E\big)}{\big(E' - E^{(0)}_B\big)\big(E - E^{(0)}_A\big)} F_A F_B \sum_P (-1)^P \sum_n \Bigg\{ \frac{\langle Pb_2|R_{f_1}|n\rangle\langle n|R_{f_2}|a_2\rangle \delta_{Pb_1a_1}}{E' - \varepsilon_{a_1} + k^0_{f_1} - \varepsilon_n} \\
&+ \frac{\langle Pb_1|R_{f_1}|n\rangle\langle n|R_{f_2}|a_1\rangle \delta_{Pb_2a_2}}{E' - \varepsilon_{a_2} + k^0_{f_1} - \varepsilon_n} + (f_1 \leftrightarrow f_2) \Bigg\}\,,
\end{aligned} \tag{17}$$

where R_f is the transition operator, $R_f = e\alpha_\nu A^{\nu *}_f$, $\alpha^\mu = \gamma^0\gamma^\mu = (1,\boldsymbol{\alpha})$, $E^{(0)}_A = \varepsilon_{a_1} + \varepsilon_{a_2}$, and $E^{(0)}_B = \varepsilon_{b_1} + \varepsilon_{b_2}$, and $u = 1 - i0$ preserves the proper treatment of poles of the electron propagators; the shorthand notation $(f_1 \leftrightarrow f_2)$ stands for the contributions with interchanged photons f_1 and f_2. Substituting this expression into Eq. (16) and integrating over E and E', one obtains

$$\tau^{(0)}_{\gamma_{f_1},\gamma_{f_2},B;A} = -F_A F_B \sum_P (-1)^P \sum_n \left\{ \frac{\langle Pb_2|R_{f_1}|n\rangle\langle n|R_{f_2}|a_2\rangle \delta_{Pb_1a_1}}{\varepsilon_{Pb_2} + k^0_{f_1} - \varepsilon_n} + \frac{\langle Pb_1|R_{f_1}|n\rangle\langle n|R_{f_2}|a_1\rangle \delta_{Pb_2a_2}}{\varepsilon_{Pb_1} + k^0_{f_1} - \varepsilon_n} + (f_1 \leftrightarrow f_2) \right\}. \tag{18}$$

The corresponding differential transition probability is given by

$$dW^{(0)}_{B;A}\big(k_{f_1},\epsilon_{f_1},k_{f_2},\epsilon_{f_2}\big) = 2\pi \big|\tau^{(0)}_{\gamma_{f_1},\gamma_{f_2},B;A}\big|^2 \delta\big(E^{(0)}_B + k^0_{f_1} + k^0_{f_2} - E^{(0)}_A\big) d\mathbf{k}_{f_1} d\mathbf{k}_{f_2}\,. \tag{19}$$

Summing over the photon polarizations and integrating over the photon energies and angles, one obtains the total decay rate

$$W^{(0)}_{B;A} = \frac{1}{2}\int_0^{\Delta^{(0)}_{AB}} dk^0_{f_1}\,(k^0_{f_1})^2\big(\Delta^{(0)}_{AB} - k^0_{f_1}\big)^2\,2\pi \sum_{\epsilon_{f_1},\epsilon_{f_2}} \int d\Omega_{k_{f_1}} d\Omega_{k_{f_2}} \big|\tau^{(0)}_{\gamma_{f_1},\gamma_{f_2},B;A}\big|^2 , \tag{20}$$

where $\Delta^{(0)}_{AB} = E^{(0)}_A - E^{(0)}_B$. Equations (19) and (20) together with Eq. (18) describe the zeroth-order differential and total two-photon transition probabilities, respectively. They coincide with the corresponding formulas employed for the calculation of the two-photon decay rates in He-like ions [2,10,11,36] in the independent particle model approximation.

B. First-order interelectronic-interaction correction

With the formalism outlined above, we are ready now to derive the first-order interelectronic-interaction corrections to the two-photon transition amplitude, which are defined by diagrams depicted in Fig. 2. According to Eq. (11), we start from

$$S^{(1)}_{\gamma_{f_1},\gamma_{f_2},B;A} = \delta(E_B + k^0_{f_1} + k^0_{f_2} - E_A)\left[\oint_{\Gamma_B} dE' \oint_{\Gamma_A} dE\, g^{(1)}_{\gamma_{f_1},\gamma_{f_2},B;A}\big(E',E,k^0_{f_1}\big) - \frac{1}{2}\oint_{\Gamma_B} dE' \oint_{\Gamma_A} dE\, g^{(0)}_{\gamma_{f_1},\gamma_{f_2},B;A}\big(E',E,k^0_{f_1}\big) \times \left(\frac{1}{2\pi i}\oint_{\Gamma_A} dE\, g^{(1)}_{AA}(E) + \frac{1}{2\pi i}\oint_{\Gamma_B} dE\, g^{(1)}_{BB}(E)\right)\right], \tag{21}$$

where $g^{(1)}_{AA}$ and $g^{(1)}_{BB}$ are defined by the first-order interelectronic-interaction diagram depicted in Fig. 3. Let us first consider the contribution of the diagrams shown in Fig. 2(a). According to the Feynman rules, we obtain

$$\begin{aligned}
&g^{(1A)}_{\gamma_{f_1},\gamma_{f_2},B;A}\big(E',E,k^0_{f_1}\big)\delta\big(E' + k^0_{f_1} + k^0_{f_2} - E\big) \\
&\quad = \left(\frac{i}{2\pi}\right)^3 F_A F_B \sum_P (-1)^P \int_{-\infty}^{\infty} dp^0_1 dp^0_2 dp'^0_1 dp'^0_2 dq^0_1 dq^0_2 d\omega\, \delta\big(E - p^0_1 - p^0_2\big)\delta\big(E' - p'^0_1 - p'^0_2\big) \\
&\qquad \times \sum_{n_1,n_2}\left\{\frac{\delta\big(p'^0_2 + k^0_{f_1} - q^0_1\big)\delta\big(q^0_1 + k^0_{f_2} - q^0_2\big)\delta\big(q^0_2 - \omega - p^0_2\big)\delta\big(p'^0_1 + \omega - p^0_1\big)}{\big(p'^0_1 - u\varepsilon_{Pb_1}\big)\big(p'^0_2 - u\varepsilon_{Pb_2}\big)\big(p^0_1 - u\varepsilon_{a_1}\big)\big(p^0_2 - u\varepsilon_{a_2}\big)}\right. \\
&\qquad \times \frac{\langle Pb_2|R_{f_1}|n_1\rangle\langle n_1|R_{f_2}|n_2\rangle\langle Pb_1 n_2|I(\omega)|a_1 a_2\rangle}{\big(q^0_1 - u\varepsilon_{n_1}\big)\big(q^0_2 - u\varepsilon_{n_2}\big)} \\
&\qquad + \frac{\delta\big(p'^0_1 + k^0_{f_1} - q^0_1\big)\delta\big(q^0_1 + k^0_{f_2} - q^0_2\big)\delta\big(q^0_2 - \omega - p^0_1\big)\delta\big(p'^0_2 + \omega - p^0_2\big)}{\big(p'^0_1 - u\varepsilon_{Pb_1}\big)\big(p'^0_2 - u\varepsilon_{Pb_2}\big)\big(p^0_1 - u\varepsilon_{a_1}\big)\big(p^0_2 - u\varepsilon_{a_2}\big)} \\
&\qquad \left.\times \frac{\langle Pb_1|R_{f_1}|n_1\rangle\langle n_1|R_{f_2}|n_2\rangle\langle n_2 Pb_2|I(\omega)|a_1 a_2\rangle}{\big(q^0_1 - u\varepsilon_{n_1}\big)\big(q^0_2 - u\varepsilon_{n_2}\big)} + (f_1 \leftrightarrow f_2)\right\},
\end{aligned} \tag{22}$$

where $I(\omega) = e^2\alpha^\mu\alpha^\nu D_{\mu\nu}(\omega)$, and $D_{\mu\nu}(\omega)$ is the photon propagator. Equation (22) is conveniently divided into irreducible and reducible parts. The reducible part is the one with $\varepsilon_{Pb_1} + \varepsilon_{n_2} = E^{(0)}_A$ in first term and with $\varepsilon_{Pb_2} + \varepsilon_{n_2} = E^{(0)}_A$ in the second term. The irreducible part is the reminder. Thus, we obtain for the irreducible contribution

$$\begin{aligned}
g^{(1A,\mathrm{irr})}_{\gamma_{f_1},\gamma_{f_2},B;A}\big(E',E,k^0_{f_1}\big) &= \left(\frac{i}{2\pi}\right)^3 F_A F_B \sum_P (-1)^P \int_{-\infty}^{\infty} dp^0 dp'^0 \frac{1}{\big(E' - E^{(0)}_B\big)\big(E - E^{(0)}_A\big)} \\
&\quad \times \left\{\sum_{n_1,n_2}^{\varepsilon_{Pb_1}+\varepsilon_{n_2}\neq E^{(0)}_A}\left(\frac{1}{p^0 - u\varepsilon_{a_1}} + \frac{1}{E - p^0 - u\varepsilon_{a_2}}\right)\left(\frac{1}{p'^0 - u\varepsilon_{Pb_1}} + \frac{1}{E' - p'^0 - u\varepsilon_{Pb_2}}\right)\right. \\
&\quad \times \frac{\langle Pb_2|R_{f_1}|n_1\rangle\langle n_1|R_{f_2}|n_2\rangle\langle Pb_1 n_2|I(p^0 - p'^0)|a_1 a_2\rangle}{\big(E' - p'^0 + k^0_{f_1} - u\varepsilon_{n_1}\big)\big(E - p'^0 - u\varepsilon_{n_2}\big)} \\
&\quad + \sum_{n_1,n_2}^{\varepsilon_{Pb_2}+\varepsilon_{n_2}\neq E^{(0)}_A}\left(\frac{1}{p^0 - u\varepsilon_{a_2}} + \frac{1}{E - p^0 - u\varepsilon_{a_1}}\right)\left(\frac{1}{p'^0 - u\varepsilon_{Pb_2}} + \frac{1}{E' - p'^0 - u\varepsilon_{Pb_1}}\right) \\
&\quad \left.\times \frac{\langle Pb_1|R_{f_1}|n_1\rangle\langle n_1|R_{f_2}|n_2\rangle\langle n_2 Pb_2|I(p^0 - p'^0)|a_1 a_2\rangle}{\big(E' - p'^0 + k^0_{f_1} - u\varepsilon_{n_1}\big)\big(E - p'^0 - u\varepsilon_{n_2}\big)} + (f_1 \leftrightarrow f_2)\right\},
\end{aligned} \tag{23}$$

and for the corresponding reducible one

$$
\begin{aligned}
g^{(1A,\mathrm{red})}_{\gamma_{f_1},\gamma_{f_2},B;A}\big(E',E,k^0_{f_1}\big) &= \left(\frac{i}{2\pi}\right)^3 F_A F_B \sum_P (-1)^P \int_{-\infty}^{\infty} dp^0 dp'^0 \frac{1}{\big(E'-E^{(0)}_B\big)\big(E-E^{(0)}_A\big)} \\
&\times \Bigg\{ \sum_{n_1,n_2}^{\varepsilon_{Pb_1}+\varepsilon_{n_2}=E^{(0)}_A} \left(\frac{1}{p^0-u\varepsilon_{a_1}}+\frac{1}{E-p^0-u\varepsilon_{a_2}}\right)\Bigg[\frac{1}{E-E^{(0)}_A}\left(\frac{1}{p'^0-u\varepsilon_{Pb_1}}+\frac{1}{E-p'^0-u\varepsilon_{n_2}}\right) \\
&+ \frac{1}{(E'-p'^0-u\varepsilon_{Pb_2})(E-p'^0-u\varepsilon_{n_2})}\Bigg]\frac{\langle Pb_2|R_{f_1}|n_1\rangle\langle n_1|R_{f_2}|n_2\rangle\langle Pb_1n_2|I(p^0-p'^0)|a_1a_2\rangle}{E'-p'^0+k^0_{f_1}-u\varepsilon_{n_1}} \\
&+ \sum_{n_1,n_2}^{\varepsilon_{Pb_2}+\varepsilon_{n_2}=E^{(0)}_A} \left(\frac{1}{p^0-u\varepsilon_{a_2}}+\frac{1}{E-p^0-u\varepsilon_{a_1}}\right)\Bigg[\frac{1}{E-E^{(0)}_A}\left(\frac{1}{p'^0-u\varepsilon_{Pb_2}}+\frac{1}{E-p'^0-u\varepsilon_{n_2}}\right) \\
&+ \frac{1}{\big(E'-p'^0-u\varepsilon_{Pb_1}\big)\big(E-p'^0-u\varepsilon_{n_2}\big)}\Bigg]\frac{\langle Pb_1|R_{f_1}|n_1\rangle\langle n_1|R_{f_2}|n_2\rangle\langle n_2Pb_2|I(p^0-p'^0)|a_1a_2\rangle}{E'-p'^0+k^0_{f_1}-u\varepsilon_{n_1}} + (f_1\leftrightarrow f_2)\Bigg\}. \qquad (24)
\end{aligned}
$$

The expression in the curly brackets in Eq. (23) is a regular function of E or E' when $E\approx E^{(0)}_A$ and $E'\approx E^{(0)}_B$. Substituting Eq. (23) into Eq. (21) and integrating over E and E', we find

$$
\begin{aligned}
\tau^{(1A,\mathrm{irr})}_{\gamma_{f_1},\gamma_{f_2},B;A} &= -F_A F_B \sum_P (-1)^P \Bigg\{ \sum_{n_1,n_2}^{\varepsilon_{Pb_1}+\varepsilon_{n_2}\neq E^{(0)}_A} \frac{\langle Pb_2|R_{f_1}|n_1\rangle\langle n_1|R_{f_2}|n_2\rangle\langle Pb_1n_2|I\big(\varepsilon_{a_1}-\varepsilon_{Pb_1}\big)|a_1a_2\rangle}{\big(\varepsilon_{Pb_2}+k^0_{f_1}-\varepsilon_{n_1}\big)\big(E^{(0)}_A-\varepsilon_{Pb_1}-\varepsilon_{n_2}\big)} \\
&+ \sum_{n_1,n_2}^{\varepsilon_{Pb_2}+\varepsilon_{n_2}\neq E^{(0)}_A} \frac{\langle Pb_1|R_{f_1}|n_1\rangle\langle n_1|R_{f_2}|n_2\rangle\langle n_2Pb_2|I\big(\varepsilon_{a_2}-\varepsilon_{Pb_2}\big)|a_1a_2\rangle}{\big(\varepsilon_{Pb_1}+k^0_{f_1}-\varepsilon_{n_1}\big)\big(E^{(0)}_A-\varepsilon_{Pb_2}-\varepsilon_{n_2}\big)} + (f_1\leftrightarrow f_2)\Bigg\}. \qquad (25)
\end{aligned}
$$

A similar calculation for the diagrams shown in Figs. 2(b)–2(d) yields

$$
\begin{aligned}
\tau^{(1B)}_{\gamma_{f_1},\gamma_{f_2},B;A} &= -F_A F_B \sum_P (-1)^P \Bigg\{ \sum_{n_1,n_2} \frac{\langle Pb_2|R_{f_1}|n_1\rangle\langle Pb_1n_1|I\big(\varepsilon_{a_1}-\varepsilon_{Pb_1}\big)|a_1n_2\rangle\langle n_2|R_{f_2}|a_2\rangle}{\big(\varepsilon_{Pb_2}+k^0_{f_1}-\varepsilon_{n_1}\big)\big(E^{(0)}_B-\varepsilon_{a_1}+k^0_{f_1}-\varepsilon_{n_2}\big)} \\
&+ \sum_{n_1,n_2} \frac{\langle Pb_1|R_{f_1}|n_1\rangle\langle n_1Pb_2|I\big(\varepsilon_{a_2}-\varepsilon_{Pb_2}\big)|n_2a_2\rangle\langle n_2|R_{f_2}|a_1\rangle}{\big(\varepsilon_{Pb_1}+k^0_{f_1}-\varepsilon_{n_1}\big)\big(E^{(0)}_B-\varepsilon_{a_2}+k^0_{f_1}-\varepsilon_{n_2}\big)} + (f_1\leftrightarrow f_2)\Bigg\}, \qquad (26)
\end{aligned}
$$

$$
\begin{aligned}
\tau^{(1C,\mathrm{irr})}_{\gamma_{f_1},\gamma_{f_2},B;A} &= -F_A F_B \sum_P (-1)^P \Bigg\{ \sum_{n_1,n_2}^{\varepsilon_{a_1}+\varepsilon_{n_1}\neq E^{(0)}_B} \frac{\langle Pb_1Pb_2|I\big(\varepsilon_{a_1}-\varepsilon_{Pb_1}\big)|a_1n_1\rangle\langle n_1|R_{f_1}|n_2\rangle\langle n_2|R_{f_2}|a_2\rangle}{\big(E^{(0)}_B-\varepsilon_{a_1}-\varepsilon_{n_1}\big)\big(E^{(0)}_B-\varepsilon_{a_1}+k^0_{f_1}-\varepsilon_{n_2}\big)} \\
&+ \sum_{n_1,n_2}^{\varepsilon_{a_2}+\varepsilon_{n_1}\neq E^{(0)}_B} \frac{\langle Pb_1Pb_2|I\big(\varepsilon_{a_2}-\varepsilon_{Pb_2}\big)|n_1a_2\rangle\langle n_1|R_{f_1}|n_2\rangle\langle n_2|R_{f_2}|a_1\rangle}{\big(E^{(0)}_B-\varepsilon_{a_2}-\varepsilon_{n_1}\big)\big(E^{(0)}_B-\varepsilon_{a_2}+k^0_{f_1}-\varepsilon_{n_2}\big)} + (f_1\leftrightarrow f_2)\Bigg\}, \qquad (27)
\end{aligned}
$$

$$
\begin{aligned}
\tau^{(1D)}_{\gamma_{f_1},\gamma_{f_2},B;A} &= -F_A F_B \sum_P (-1)^P \Bigg\{ \sum_{n_1,n_2} \frac{\langle Pb_1|R_{f_1}|n_1\rangle\langle Pb_2|R_{f_2}|n_2\rangle\langle n_1n_2|I\big(\varepsilon_{a_1}-\varepsilon_{Pb_1}-k^0_{f_1}\big)|a_1a_2\rangle}{\big(\varepsilon_{Pb_1}+k^0_{f_1}-\varepsilon_{n_1}\big)\big(E^{(0)}_A-\varepsilon_{Pb_1}-k^0_{f_1}-\varepsilon_{n_2}\big)} \\
&+ \sum_{n_1,n_2} \frac{\langle Pb_1|R_{f_1}|n_1\rangle\langle n_1Pb_2|I\big(\varepsilon_{a_1}-\varepsilon_{Pb_1}-k^0_{f_1}\big)|a_1n_2\rangle\langle n_2|R_{f_2}|a_2\rangle}{\big(\varepsilon_{Pb_1}+k^0_{f_1}-\varepsilon_{n_1}\big)\big(E^{(0)}_B-\varepsilon_{a_1}+k^0_{f_1}-\varepsilon_{n_2}\big)} \\
&+ \sum_{n_1,n_2} \frac{\langle Pb_1Pb_2|I\big(\varepsilon_{a_1}-\varepsilon_{Pb_1}-k^0_{f_1}\big)|n_1n_2\rangle\langle n_1|R_{f_1}|a_1\rangle\langle n_2|R_{f_2}|a_2\rangle}{\big(\varepsilon_{a_1}-k^0_{f_1}-\varepsilon_{n_1}\big)\big(E^{(0)}_B-\varepsilon_{a_1}+k^0_{f_1}-\varepsilon_{n_2}\big)} \\
&+ \sum_{n_1,n_2} \frac{\langle Pb_2|R_{f_2}|n_2\rangle\langle Pb_1n_2|I\big(\varepsilon_{a_1}-\varepsilon_{Pb_1}-k^0_{f_1}\big)|n_1a_2\rangle\langle n_1|R_{f_1}|a_1\rangle}{\big(\varepsilon_{a_1}-k^0_{f_1}-\varepsilon_{n_1}\big)\big(E^{(0)}_A-\varepsilon_{Pb_1}-k^0_{f_1}-\varepsilon_{n_2}\big)} + (f_1\leftrightarrow f_2)\Bigg\}. \qquad (28)
\end{aligned}
$$

In the case under consideration, only the diagrams depicted in Figs. 2(a) and 2(c) possess reducible parts. For the reducible contribution coming from the Fig. 2(a) diagrams, we have

$$\tau^{(1A,\mathrm{red})}_{\gamma_{f_1},\gamma_{f_2},B;A} = F_A F_B \sum_P (-1)^P \sum_n \left\{ \frac{\langle Pb_2|R_{f_2}|n\rangle\langle n|R_{f_1}|a_2\rangle\delta_{Pb_1a_1}}{\left(\varepsilon_{a_2}-k^0_{f_1}-\varepsilon_n\right)^2} + \frac{\langle Pb_1|R_{f_2}|n\rangle\langle n|R_{f_1}|a_1\rangle\delta_{Pb_2a_2}}{\left(\varepsilon_{a_1}-k^0_{f_1}-\varepsilon_n\right)^2} \right\} \Delta E^{(1)}_A$$
$$-\frac{i}{2\pi}\tau^{(0)}_{\gamma_{f_1},\gamma_{f_2},B;A} F_{A'}F_{A''}\int_{-\infty}^{\infty} dp^0 \left[\frac{\langle a'_1a'_2|I(p^0)|a''_1a''_2\rangle}{(p^0+i0)^2} - \frac{\langle a'_2a'_1|I(p^0)|a''_1a''_2\rangle}{(p^0-\Delta_A+i0)^2} \right], \tag{29}$$

where $\Delta E^{(1)}_A = F_{A'}F_{A''}\sum_P (-1)^P \langle Pa'_1 Pa'_2|I(\varepsilon_{Pa'_1}-\varepsilon_{a''_1})|a''_1a''_2\rangle$ is the one-photon exchange correction to the state A and $\Delta_A = \varepsilon_{a_2}-\varepsilon_{a_1}$. Combining this term with the reducible part of the Fig. 2(c) diagrams and with the second term in formula (21), we obtain the total reducible contribution:

$$\tau^{(1,\mathrm{red})}_{\gamma_{f_1},\gamma_{f_2},B;A} = F_A F_B \sum_P (-1)^P \sum_n \left\{ \frac{\langle Pb_2|R_{f_1}|n\rangle\langle n|R_{f_2}|a_2\rangle\delta_{Pb_1a_1}}{\left(\varepsilon_{Pb_2}+k^0_{f_1}-\varepsilon_n\right)^2}\Delta E^{(1)}_B + \frac{\langle Pb_1|R_{f_1}|n\rangle\langle n|R_{f_2}|a_1\rangle\delta_{Pb_2a_2}}{\left(\varepsilon_{Pb_1}+k^0_{f_1}-\varepsilon_n\right)^2}\Delta E^{(1)}_B \right.$$
$$\left. + \frac{\langle Pb_2|R_{f_2}|n\rangle\langle n|R_{f_1}|a_2\rangle\delta_{Pb_1a_1}}{\left(\varepsilon_{a_2}-k^0_{f_1}-\varepsilon_n\right)^2}\Delta E^{(1)}_A + \frac{\langle Pb_1|R_{f_2}|n\rangle\langle n|R_{f_1}|a_1\rangle\delta_{Pb_2a_2}}{\left(\varepsilon_{a_1}-k^0_{f_1}-\varepsilon_n\right)^2}\Delta E^{(1)}_A \right\}$$
$$+\frac{1}{2}\tau^{(0)}_{\gamma_{f_1},\gamma_{f_2},B;A}[F_{A'}F_{A''}\langle a'_2a'_1|I'(\Delta_A)|a''_1a''_2\rangle + F_{B'}F_{B''}\langle b'_2b'_1|I'(\Delta_B)|b''_1b''_2\rangle], \tag{30}$$

where $\Delta E^{(1)}_B$ and Δ_B are defined similar to $\Delta E^{(1)}_A$ and Δ_A, $I'(\Delta) = [dI(\omega)/d\omega]_{\omega=\Delta}$. The final expression for $\tau^{(1)}_{\gamma_{f_1},\gamma_{f_2},B;A}$ is given by the sum of Eqs. (25)–(28) and (30):

$$\tau^{(1)}_{\gamma_{f_1},\gamma_{f_2},B;A} = \tau^{(1A,\mathrm{irr})}_{\gamma_{f_1},\gamma_{f_2},B;A} + \tau^{(1B)}_{\gamma_{f_1},\gamma_{f_2},B;A} + \tau^{(1C,\mathrm{irr})}_{\gamma_{f_1},\gamma_{f_2},B;A} + \tau^{(1D)}_{\gamma_{f_1},\gamma_{f_2},B;A} + \tau^{(1,\mathrm{red})}_{\gamma_{f_1},\gamma_{f_2},B;A}. \tag{31}$$

Finally, the first-order interelectronic-interaction corrections to the differential and total transition probabilities can be expressed according to the following equations:

$$dW^{(1)}_{B;A}(k_{f_1},\epsilon_{f_1},k_{f_2},\epsilon_{f_2}) = 4\pi\,\mathrm{Re}\{\tau^{(0)*}_{\gamma_{f_1},\gamma_{f_2},B;A}\tau^{(1)}_{\gamma_{f_1},\gamma_{f_2},B;A}\}\delta(E^{(1)}_B + k^0_{f_1} + k^0_{f_2} - E^{(1)}_A)d\mathbf{k}_{f_1}d\mathbf{k}_{f_2}$$
$$+\Delta dW^{(0)}_{B;A}(k_{f_1},\epsilon_{f_1},k_{f_2},\epsilon_{f_2}), \tag{32}$$

$$W^{(1)}_{B;A} = \frac{1}{2}\int_0^{\Delta^{(1)}_{AB}} dk^0_{f_1}\,(k^0_{f_1})^2(\Delta^{(1)}_{AB}-k^0_{f_1})^2\,4\pi\sum_{\epsilon_{f_1},\epsilon_{f_2}}\int d\Omega_{k_{f_1}}d\Omega_{k_{f_2}}\mathrm{Re}\{\tau^{(0)*}_{\gamma_{f_1},\gamma_{f_2},B;A}\tau^{(1)}_{\gamma_{f_1},\gamma_{f_2},B;A}\} + \Delta W^{(0)}_{B;A}, \tag{33}$$

where $E^{(1)}_A = E^{(0)}_A + \Delta E^{(1)}_A$, $E^{(1)}_B = E^{(0)}_B + \Delta E^{(1)}_B$, $\Delta^{(1)}_{AB} = E^{(1)}_A - E^{(1)}_B$, and

$$\Delta dW^{(0)}_{B;A}(k_{f_1},\epsilon_{f_1},k_{f_2},\epsilon_{f_2}) = 2\pi|\tau^{(0)}_{\gamma_{f_1},\gamma_{f_2},B;A}|^2\delta(E^{(1)}_B + k^0_{f_1} + k^0_{f_2} - E^{(1)}_A)d\mathbf{k}_{f_1}d\mathbf{k}_{f_2} - dW^{(0)}_{B;A}(k_{f_1},\epsilon_{f_1},k_{f_2},\epsilon_{f_2}), \tag{34}$$

$$\Delta W^{(0)}_{B;A} = \frac{1}{2}\int_0^{\Delta^{(1)}_{AB}} dk^0_{f_1}\,(k^0_{f_1})^2(\Delta^{(1)}_{AB}-k^0_{f_1})^2\,2\pi\sum_{\epsilon_{f_1},\epsilon_{f_2}}\int d\Omega_{k_{f_1}}d\Omega_{k_{f_2}}|\tau^{(0)}_{\gamma_{f_1},\gamma_{f_2},B;A}|^2 - W^{(0)}_{B;A} \tag{35}$$

are the contributions originating from changing the transition energy $\Delta^{(0)}_{AB}$ in the zeroth-order transition probability to the energy $\Delta^{(1)}_{AB}$, which accounts for the interelectronic-interaction correction.

C. First-order interelectronic-interaction correction with screening potential

In the preceding subsection, we presented the formulas for the first-order interelectronic-interaction correction involving electron states and propagators in the external Coulomb potential of the nucleus as the zeroth-order approximation (the original Furry picture). Now we consider an extended Furry picture, which includes a local screening potential in the unperturbed Hamiltonian. Since we consider the two-photon decays from the single-excited state to the ground state of He-like ions, we construct the screening potential for the initial state A such that it takes into account partly the interelectronic interaction between the electrons a_2 and a_1. By employing the extended Furry representation, we relieve the quasidegeneracy of the $(1s2s)_J$ and $(1s2p_{1/2})_J$ states already at the zeroth-order level, and we improve the energy level scheme of the first excited states in high-Z heavy ions. Two different local screening potentials V_{scr} are used: the Kohn-Sham potential and the core-Hartree potential. Both potentials were successfully incorporated in previous calculations [11,19,37,38].

In the extended Furry picture, we solve the Dirac equation with an effective spherically symmetric potential treating the interaction with the external Coulomb potential of the nucleus and the local screening potential exact to all orders. The electron propagators in Figs. 1–3 have to be treated in the effective potential (we indicate this diagrammatically via the triple electron line). The formulas derived in the previous subsection remain formally the same, but keeping in mind that the Dirac spectrum is now generated by solving the Dirac equation with the effective potential. However, additional counterterm diagrams with the extra interaction term $-V_{\rm scr}$ arise. In Figs. 4 and 5, the additional diagrams are depicted, where the extra interaction term $-V_{\rm scr}$ is represented graphically by the symbol $\otimes$. Thus, according to the Feynman rules we derive the expressions for the counterterm diagrams shown in Figs. 4(a)–4(c),

$$\tau^{(1A,\mathrm{irr})\mathrm{ext}}_{\gamma_{f_1},\gamma_{f_2},B;A} = F_A F_B \sum_P (-1)^P \left\{ \sum_{n_1,n_2}^{\varepsilon_{n_2}\neq\varepsilon_{a_2}} \frac{\langle Pb_2|R_{f_1}|n_1\rangle\langle n_1|R_{f_2}|n_2\rangle\langle n_2|V_{\rm scr}|a_2\rangle\delta_{Pb_1a_1}}{\left(\varepsilon_{Pb_2}+k^0_{f_1}-\varepsilon_{n_1}\right)\left(\varepsilon_{a_2}-\varepsilon_{n_2}\right)} \right.$$
$$\left. + \sum_{n_1,n_2}^{\varepsilon_{n_2}\neq\varepsilon_{a_1}} \frac{\langle Pb_1|R_{f_1}|n_1\rangle\langle n_1|R_{f_2}|n_2\rangle\langle n_2|V_{\rm scr}|a_1\rangle\delta_{Pb_2a_2}}{\left(\varepsilon_{Pb_1}+k^0_{f_1}-\varepsilon_{n_1}\right)\left(\varepsilon_{a_1}-\varepsilon_{n_2}\right)} + (f_1 \leftrightarrow f_2) \right\}, \tag{36}$$

$$\tau^{(1B)\mathrm{ext}}_{\gamma_{f_1},\gamma_{f_2},B;A} = F_A F_B \sum_P (-1)^P \left\{ \sum_{n_1,n_2} \frac{\langle Pb_2|R_{f_1}|n_1\rangle\langle n_1|V_{\rm scr}|n_2\rangle\langle n_2|R_{f_2}|a_2\rangle\delta_{Pb_1a_1}}{\left(\varepsilon_{Pb_2}+k^0_{f_1}-\varepsilon_{n_1}\right)\left(\varepsilon_{Pb_2}+k^0_{f_1}-\varepsilon_{n_2}\right)} \right.$$
$$\left. + \sum_{n_1,n_2} \frac{\langle Pb_1|R_{f_1}|n_1\rangle\langle n_1|V_{\rm scr}|n_2\rangle\langle n_2|R_{f_2}|a_1\rangle\delta_{Pb_2a_2}}{\left(\varepsilon_{Pb_1}+k^0_{f_1}-\varepsilon_{n_1}\right)\left(\varepsilon_{Pb_1}+k^0_{f_1}-\varepsilon_{n_2}\right)} + (f_1 \leftrightarrow f_2) \right\}, \tag{37}$$

$$\tau^{(1C,\mathrm{irr})\mathrm{ext}}_{\gamma_{f_1},\gamma_{f_2},B;A} = F_A F_B \sum_P (-1)^P \left\{ \sum_{n_1,n_2}^{\varepsilon_{n_1}\neq\varepsilon_{Pb_2}} \frac{\langle Pb_2|V_{\rm scr}|n_1\rangle\langle n_1|R_{f_1}|n_2\rangle\langle n_2|R_{f_2}|a_2\rangle\delta_{Pb_1a_1}}{\left(\varepsilon_{Pb_2}-\varepsilon_{n_1}\right)\left(\varepsilon_{Pb_2}+k^0_{f_1}-\varepsilon_{n_2}\right)} \right.$$
$$\left. + \sum_{n_1,n_2}^{\varepsilon_{n_1}\neq\varepsilon_{Pb_1}} \frac{\langle Pb_1|V_{\rm scr}|n_1\rangle\langle n_1|R_{f_1}|n_2\rangle\langle n_2|R_{f_2}|a_1\rangle\delta_{Pb_2a_2}}{\left(\varepsilon_{Pb_1}-\varepsilon_{n_1}\right)\left(\varepsilon_{Pb_1}+k^0_{f_1}-\varepsilon_{n_2}\right)} + (f_1 \leftrightarrow f_2) \right\}. \tag{38}$$

For the additional reducible contribution, we obtain

$$\tau^{(1,\mathrm{red})\mathrm{ext}}_{\gamma_{f_1},\gamma_{f_2},B;A} = -F_A F_B \sum_P (-1)^P \sum_n \left\{ \left[\frac{\langle Pb_2|R_{f_1}|n\rangle\langle n|R_{f_2}|a_2\rangle\delta_{Pb_1a_1}}{\left(\varepsilon_{Pb_2}+k^0_{f_1}-\varepsilon_n\right)^2} + \frac{\langle Pb_1|R_{f_1}|n\rangle\langle n|R_{f_2}|a_1\rangle\delta_{Pb_2a_2}}{\left(\varepsilon_{Pb_1}+k^0_{f_1}-\varepsilon_n\right)^2} \right] \Delta E^{(1)\mathrm{ext}}_B \right.$$
$$\left. + \left[\frac{\langle Pb_2|R_{f_2}|n\rangle\langle n|R_{f_1}|a_2\rangle\delta_{Pb_1a_1}}{\left(\varepsilon_{a_2}-k^0_{f_1}-\varepsilon_n\right)^2} + \frac{\langle Pb_1|R_{f_2}|n\rangle\langle n|R_{f_1}|a_1\rangle\delta_{Pb_2a_2}}{\left(\varepsilon_{a_1}-k^0_{f_1}-\varepsilon_n\right)^2} \right] \Delta E^{(1)\mathrm{ext}}_A \right\}, \tag{39}$$

where $\Delta E^{(1)\mathrm{ext}}_A$ and $\Delta E^{(1)\mathrm{ext}}_B$ are the counterterm contributions to the energy of the initial and final states, respectively,

$$\Delta E^{(1)\mathrm{ext}}_A = -F_{A'}F_{A''}\sum_P (-1)^P \left(\langle Pa'_1|V_{\rm scr}|a''_1\rangle\delta_{Pa'_2a''_2} + \langle Pa'_2|V_{\rm scr}|a''_2\rangle\delta_{Pa'_1a''_1}\right). \tag{40}$$

Thus, in the extended Furry representation these extra terms have to be added to the corresponding corrections to the transition amplitude as $\tau^{(1A,\mathrm{irr})}_{\gamma_{f_1},\gamma_{f_2},B;A} \to (\tau^{(1A,\mathrm{irr})}_{\gamma_{f_1},\gamma_{f_2},B;A} + \tau^{(1A,\mathrm{irr})\mathrm{ext}}_{\gamma_{f_1},\gamma_{f_2},B;A})$, and, similarly, the remaining terms. Moreover, in Eqs. (32) and (33) the employed energies $E^{(1)}_A$ and $E^{(1)}_B$ have to be corrected to the counterterm contributions $E^{(1)}_A = E^{(0)}_A + \Delta E^{(1)}_A + \Delta E^{(1)\mathrm{ext}}_A$ and $E^{(1)}_B = E^{(0)}_B + \Delta E^{(1)}_B + \Delta E^{(1)\mathrm{ext}}_B$.

III. NUMERICAL RESULTS AND DISCUSSION

Now let us turn to the presentation and discussion of our numerical results for the two-photon transitions $2\,^1S_0 \to 1\,^1S_0$ and $2\,^3S_1 \to 1\,^1S_0$ in He-like ions. The infinite summations over the complete Dirac spectrum involved in the numerical evaluations are performed employing the finite-basis set method. The B-splines basis set was constructed utilizing the dual kinetic balance approach [39]. The homogeneously charged sphere model for the nuclear charge distribution is

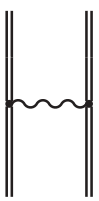

FIG. 3. One-photon exchange diagram. The photon propagator is represented by the wavy line.

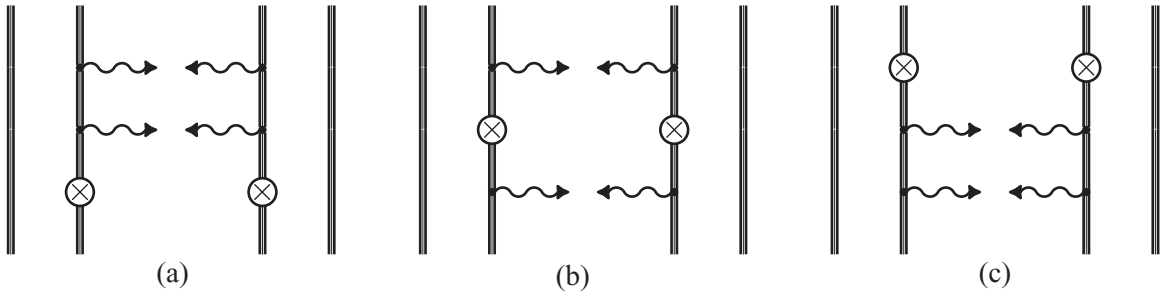

FIG. 4. The counterterm diagrams for the first-order interelectronic-interaction corrections to the two-photon emission. The triple lines describe the electron propagators in the effective potential. The symbol ⊗ represents the extra interaction term associated with the local screening potential.

employed together with the rms radii taken from Ref. [40], except for the thorium and uranium ions, for which the recent rms values are taken from Ref. [41]. The Kohn-Sham and core-Hartree screening potentials are employed in the zeroth-order approximation. The Kohn-Sham potentials are constructed for the $2\,^1S_0$ state in the case of the $2\,^1S_0 \to 1\,^1S_0$ transition, and for the $2\,^3S_1$ state in the case of the $2\,^3S_1 \to 1\,^1S_0$ transition, while the core-Hartree potential is just a Coulomb potential generated by the $1s$ electron. The screening potentials are generated self-consistently by solving the Dirac equation until the energies of the core and valence states become stable on the level of 10^{-9}. In our final compilation, we employ the Kohn-Sham potential as a starting one, since the transition energies are better reproduced in this case. The gauge invariance serves as an accurate check of consistency of the derived formulas and the numerical procedure. We analytically prove the gauge invariance of the obtained formulas. To separate out the proper gauge invariant first-order contribution, we replace the transition operator R_{f_2} with the first two terms of the Taylor expansion in $\tau^{(0)}_{\gamma_{f_1},\gamma_{f_2},B;A}$, as $R_{f_2}(k^0_{f_2}) \simeq R_{f_2}(\Delta^{(0)}_{AB} - k^0_{f_1}) + R'_{f_2}(\Delta^{(0)}_{AB} - k^0_{f_1}) \times [\Delta E^{(1)}_A - \Delta E^{(1)}_B]$, and with the first term only in $\tau^{(1)}_{\gamma_{f_1},\gamma_{f_2},B;A}$, as $R_{f_2}(k^0_{f_2}) \simeq R_{f_2}(\Delta^{(0)}_{AB} - k^0_{f_1})$. In the numerical procedure, we employ the Feynman and Coulomb gauges for the photon propagator and the velocity and length gauges for the emitted photons, and we demonstrate the gauge independence of the final results. In Table I, we present the numerical results for the individual contributions evaluated in the different gauges for He-like thorium. As one can see from the table, the gauge invariance is restored in the final values. A detailed discussion of these questions will be presented elsewhere.

In Table II, we present the zeroth-order and final values of the two-photon decay rates for the transitions $2\,^1S_0 \to 1\,^1S_0 + 2\gamma(\mathrm{E1})$ and $2\,^3S_1 \to 1\,^1S_0 + 2\gamma(\mathrm{E1})$ in He-like ions. These results include only the dominant 2E1 channel of the two-photon decay. The final results for the total two-photon decay rates are evaluated according to the following formula:

$$W_{B;A} = \frac{1}{2}\int_0^{\Delta^{(1)}_{AB}} dk^0_{f_1}\,\left(k^0_{f_1}\right)^2\left(\Delta^{(1)}_{AB} - k^0_{f_1}\right)^2 2\pi \times \sum_{\epsilon_{f_1},\epsilon_{f_2}} \int d\Omega_{k_{f_1}} d\Omega_{k_{f_2}} \left|\tau^{(0)}_{\gamma_{f_1},\gamma_{f_2},B;A} + \tau^{(1)}_{\gamma_{f_1},\gamma_{f_2},B;A}\right|^2 \tag{41}$$

where in $\tau^{(0)}_{\gamma_{f_1},\gamma_{f_2},B;A}$ and $\tau^{(1)}_{\gamma_{f_1},\gamma_{f_2},B;A}$, defined by Eq. (18) and Eqs. (31) and (36)–(39), respectively, we separate out the terms up to first order. The transition energies $\Delta^{(1)}_{AB}$ together with the transition amplitudes $\tau^{(1)}_{\gamma_{f_1},\gamma_{f_2},B;A}$ consistently include the first-order interelectronic-interaction corrections to the two-photon decay rate $W_{B;A}$. However, for high-Z ions it is important also to take into account the radiative corrections. In the framework of QED perturbation theory, one has to evaluate radiative corrections to both the transition energy and the transition amplitude. To account partially for the radiative corrections, we employ the more accurate transition energies taken from Ref. [42] for the transition energies $\Delta^{(1)}_{AB}$ in the upper integral limit and in the factor $(\Delta^{(1)}_{AB} - k^0_{f_1})$ in Eq. (41). Including in this way the more accurate transition energies does not violate the gauge invariance of the result, it just scales the decay rates to another value of the transition energy. The employment of the more accurate transition energies yields corrections that are negligible for intermediate-Z ions, which, however, become important for high-Z ions.

The results of calculations performed by starting with the Coulomb, core-Hartree, and Kohn-Sham potentials are presented in Table II. Comparing the zeroth-order values in the Coulomb and screening potentials, one can observe that the screening potentials account for a considerable part of electron-electron interaction effects. However, the difference between the zeroth-order results for the core-Hartree and Kohn-Sham potentials is still quite large. Accounting for the first-order interelectronic-interaction correction, we obtain the decay rates $W_{B;A}$, which depend much less on the screening potential. The remaining difference between the final values $W_{B;A}$ in the core-Hartree and Kohn-Sham potentials provides a hint for the uncertainty due to unaccounted second- and higher-order interelectronic-interaction corrections. In Table II, we also compare the obtained decay rates $W_{B;A}$ with the results

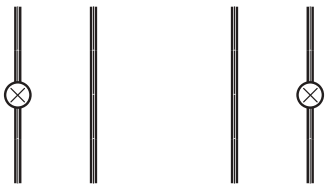

FIG. 5. The counterterm diagrams for the one-photon exchange correction. Notations are the same as in Fig. 4.

TABLE I. Individual contributions to the total two-photon decay rates for the transitions $2\,^1S_0 \to 1\,^1S_0 + 2\gamma(\mathrm{E1})$ and $2\,^3S_1 \to 1\,^1S_0 + 2\gamma(\mathrm{E1})$ in He-like $^{232}Th^{88+}$, in units s^{-1}. The Kohn-Sham potential has been used as the starting potential. The velocity and length gauges have been employed for the emitted photons, and Feynman and Coulomb gauges for the photon propagator. The more accurate transition energies $\Delta^{(1)}_{2\,^1S_0;1\,^1S_0} = 91\,531$ eV and $\Delta^{(1)}_{2\,^3S_1;1\,^1S_0} = 91\,291$ eV are taken from Ref. [42]. Numbers in brackets denote powers of 10.

Gauges	$W^{(0)}_{B;A}$	$\Delta W^{(0)}_{B;A}$	$W^{(1,\mathrm{irr})}_{B;A}$	$W^{(1,\mathrm{red})}_{B;A}$	$W_{B;A}$
		$2\,^1S_0 \to 1\,^1S_0$			
Velocity and Feynman	6.439[12]	−0.0862[12]	0.0165[12]	0.0123[12]	6.381[12]
Length and Feynman	6.439[12]	−0.1610[12]	0.0054[12]	0.0982[12]	6.381[12]
Velocity and Coulomb	6.439[12]	−0.0862[12]	0.0169[12]	0.0119[12]	6.381[12]
Length and Coulomb	6.439[12]	−0.1610[12]	0.0058[12]	0.0978[12]	6.381[12]
		$2\,^3S_1 \to 1\,^1S_0$			
Velocity and Feynman	1.686[10]	−0.0972[10]	0.0115[10]	0.0349[10]	1.636[10]
Length and Feynman	1.686[10]	−0.1746[10]	0.0369[10]	0.0868[10]	1.636[10]
Velocity and Coulomb	1.686[10]	−0.0972[10]	0.0114[10]	0.0350[10]	1.636[10]
Length and Coulomb	1.686[10]	−0.1746[10]	0.0369[10]	0.0869[10]	1.636[10]

of other theoretical calculations. In the case of the $2\,^1S_0$ state, our decay rates disagree slightly with the rates given by Derevianko and Johnson [10]. For high-Z ions, this can be explained by the radiative corrections, which are included in our transition energies. The comparison with the results obtained by Drake [2] gives a better agreement within the indicated uncertainty. In the case of the $2\,^3S_1$ state, the interelectronic interaction affects the two-photon decay rates much stronger, and therefore our accuracy becomes slightly worse. For this case, our results are in fair agreement with those values of Ref. [10].

As one can see from Table II, the final values of the total two-photon decay rates calculated with the core-Hartree and Kohn-Sham potentials are very close to each other. With this in mind, we restrict our further consideration to the calculations performed with the Kohn-Sham screening potential.

Beyond the dominant 2E1 decay channel, we consider also the higher-multipole contributions to the two-photon decay rates. In Table III, we present the contributions of higher multipoles calculated in the zeroth-order approximation. In the case of the $2\,^1S_0$ state, the contribution to the total two-photon decay rate arises only from the photons with the same multipole numbers. The correction due to the higher multipoles rapidly increases with Z, but even for $Z = 92$ it is smaller by a factor 10^3 than the dominant 2E1 decay rate. Unlike the $2\,^1S_0$ state, in the case of the two-photon $2\,^3S_1 \to 1\,^1S_0$ transition, the higher multipoles decay rates are relatively large, as was first indicated by Dunford [43]. Our results for the E1M2 decay rate are in reasonable agreement with those of Ref. [43]. Moreover, we also evaluate the 2M1 channel, which contribution becomes comparable with the E1M2 for high-Z ions. The contributions of higher multipoles are included in our final compilations.

In Table IV, we compare the theoretical and experimental two-photon decay rates of the $2\,^1S_0$ state. As one can see from the table, for Br^{33+} and Nb^{39+} ions the theory is in good agreement with the experiment, but for Ni^{26+} and

TABLE II. The zeroth-order and final values of the total two-photon decay rates (2E1 channel only) for the transitions $2\,^1S_0 \to 1\,^1S_0$ and $2\,^3S_1 \to 1\,^1S_0$ in He-like ions starting with the Coulomb, core-Hartree, and Kohn-Sham potentials, in units s^{-1}. Comparison with other theoretical calculations is also made. Numbers in brackets denote powers of 10.

	Coulomb	Core-Hartree		Kohn-Sham		Other theor.	
Z	$W^{(0)}_{B;A}$	$W^{(0)}_{B;A}$	$W_{B;A}$	$W^{(0)}_{B;A}$	$W_{B;A}$	Ref. [10]	Ref. [2]
				$2\,^1S_0 \to 1\,^1S_0$			
30	1.164[10]	9.944[09]	9.903[09]	1.006[10]	9.900[09]	9.938[09]	9.88(3)[09]
50	2.370[11]	2.163[11]	2.152[11]	2.177[11]	2.152[11]	2.164[11]	2.15(1)[11]
70	1.655[12]	1.554[12]	1.545[12]	1.560[12]	1.544[12]	1.556[12]	1.55(1)[12]
90	6.728[12]	6.421[12]	6.382[12]	6.439[12]	6.381[12]	6.439[12]	6.41(6)[12]
92	7.580[12]	7.242[12]	7.199[12]	7.262[12]	7.199[12]	7.265[12]	7.24(8)[12]
				$2\,^3S_1 \to 1\,^1S_0$			
30	9.06[05]	4.64[05]	4.15[05]	4.42[05]	4.13[05]	4.17[05]	
50	1.02[08]	7.33[07]	6.88[07]	7.16[07]	6.85[07]	6.88[07]	
70	2.13[09]	1.74[09]	1.67[09]	1.72[09]	1.66[09]	1.66[09]	
90	1.96[10]	1.70[10]	1.64[10]	1.69[10]	1.64[10]	1.63[10]	
92	2.38[10]	2.07[10]	1.99[10]	2.05[10]	1.99[10]	1.98[10]	

TABLE III. Contributions of the higher multipoles (MP) to the total two-photon decay rates included in the zeroth-order approximation, in units s^{-1}. Numbers in brackets denote powers of 10.

MP	$Z = 30$	$Z = 50$	$Z = 70$	$Z = 90$	$Z = 92$
		$2\,^1S_0 \to 1\,^1S_0$			
M1M1	1.40[04]	2.65[06]	8.56[07]	1.14[09]	1.43[09]
E2E2	4.74[03]	8.19[05]	2.33[07]	2.71[08]	3.35[08]
		$2\,^3S_1 \to 1\,^1S_0$			
E1M2	7.57[04]	1.32[07]	3.79[08]	4.51[09]	5.59[09]
		1.26[07][a]	3.62[08][a]	4.30[09][a]	5.32[09][a]
M1M1	1.58[01]	2.46[04]	3.33[06]	1.46[08]	2.05[08]

[a]Reference [43].

Kr^{34+} ions all theoretical calculations predict that the values will be slightly larger than the experimental results. In the worst case of the Kr^{34+} ion, this difference amounts to about two standard deviations.

Finally, in Table V we present our total two-photon decay rates for the transitions $2\,^1S_0 \to 1\,^1S_0$ and $2\,^3S_1 \to 1\,^1S_0$.

Besides the total decay rates, we present the spectral-distribution functions $dW_{B;A}/dy$ for the two-photon transitions $2\,^1S_0 \to 1\,^1S_0$ and $2\,^3S_1 \to 1\,^1S_0$ in Tables VI and VII, respectively. The photon energy distribution function $dW_{B;A}/dy$ expressed as a function of the reduced energy $y = k^0_{f_1}/\Delta^{(1)}_{AB}$ transported by one of the two photons reads

$$dW_{B;A}/dy = y^2(1-y)^2\left(\Delta^{(1)}_{AB}\right)^5 2\pi \times \sum_{\epsilon_{f_1},\epsilon_{f_2}} \int d\Omega_{k_{f_1}} d\Omega_{k_{f_2}} \left|\tau^{(0)}_{\gamma_{f_1},\gamma_{f_2},B;A} + \tau^{(1)}_{\gamma_{f_1},\gamma_{f_2},B;A}\right|^2, \quad (42)$$

and then the total decay rate can be found via the following equation:

$$W_{B;A} = \frac{1}{2}\int_0^1 dy\,(dW_{B;A}/dy)\,. \quad (43)$$

Since we employ the more accurate transition energy $\Delta^{(1)}_{AB}$ from Ref. [42], our energy distribution function appears to be not exactly symmetric with respect to the center point at $y = 0.5$. This asymmetry comes mainly due to the higher-order corrections included in the transition energy but neglected in the transition amplitude. In Tables VI and VII and in Figs. 6 and 7, we present the spectral-distribution functions $dW_{B;A}/dy$ calculated as a half-sum of the contributions at the points y and $1 - y$. For the $2\,^1S_0$ state, the energy distribution function has one maximum at $y = 0.5$, and in Table VI we give also the reduced full width at half maximum (FWHM) values. The behavior of the reduced FWHM values as a function of Z

TABLE V. The total two-photon decay rates for the transitions $2\,^1S_0 \to 1\,^1S_0$ and $2\,^3S_1 \to 1\,^1S_0$ in He-like ions, in units s^{-1}. The transition energies are taken from Ref. [42]. Numbers in brackets denote powers of 10.

Z	$2\,^1S_0$	$2\,^3S_1$	Z	$2\,^1S_0$	$2\,^3S_1$
28	6.493[09]	2.40[05]	61	6.948[11]	5.56[08]
29	8.048[09]	3.44[05]	62	7.640[11]	6.49[08]
30	9.900[09]	4.88[05]	63	8.388[11]	7.56[08]
31	1.209[10]	6.84[05]	64	9.193[11]	8.77[08]
32	1.467[10]	9.46[05]	65	1.006[12]	1.02[09]
33	1.769[10]	1.30[06]	66	1.099[12]	1.17[09]
34	2.121[10]	1.76[06]	67	1.199[12]	1.35[09]
35	2.529[10]	2.36[06]	68	1.307[12]	1.56[09]
36	2.999[10]	3.13[06]	69	1.422[12]	1.79[09]
37	3.539[10]	4.13[06]	70	1.545[12]	2.04[09]
38	4.158[10]	5.40[06]	71	1.676[12]	2.33[09]
39	4.863[10]	7.01[06]	72	1.816[12]	2.66[09]
40	5.664[10]	9.04[06]	73	1.966[12]	3.03[09]
41	6.572[10]	1.16[07]	74	2.125[12]	3.44[09]
42	7.595[10]	1.47[07]	75	2.294[12]	3.90[09]
43	8.747[10]	1.86[07]	76	2.474[12]	4.41[09]
44	1.004[11]	2.33[07]	77	2.665[12]	4.98[09]
45	1.148[11]	2.91[07]	78	2.867[12]	5.61[09]
46	1.310[11]	3.61[07]	79	3.082[12]	6.32[09]
47	1.489[11]	4.46[07]	80	3.309[12]	7.10[09]
48	1.688[11]	5.49[07]	81	3.549[12]	7.96[09]
49	1.908[11]	6.71[07]	82	3.803[12]	8.92[09]
50	2.152[11]	8.18[07]	83	4.071[12]	9.98[09]
51	2.420[11]	9.91[07]	84	4.353[12]	1.11[10]
52	2.715[11]	1.20[08]	85	4.650[12]	1.24[10]
53	3.039[11]	1.44[08]	86	4.963[12]	1.38[10]
54	3.394[11]	1.73[08]	87	5.292[12]	1.54[10]
55	3.783[11]	2.06[08]	88	5.638[12]	1.71[10]
56	4.206[11]	2.45[08]	89	6.002[12]	1.90[10]
57	4.668[11]	2.90[08]	90	6.383[12]	2.10[10]
58	5.171[11]	3.43[08]	91	6.782[12]	2.32[10]
59	5.716[11]	4.04[08]	92	7.200[12]	2.57[10]
60	6.308[11]	4.75[08]			

TABLE IV. Comparison of theory and experiment for the two-photon decay rates of the $2\,^1S_0$ state in He-like ions, in units s^{-1}. Numbers in brackets denote powers of 10.

Z	Expt.	This work	Ref. [10]	Ref. [2]
28	6.406(66)[09][a]	6.493[09]	6.517[09]	6.482(21)[09]
35	2.543(21)[10][b]	2.529[10]	2.540[10]	
36	2.934(30)[10][c]	2.999[10]	3.012[10]	2.993(12)[10]
41	6.52(26)[10][d]	6.572[10]	6.604[10]	

[a]Reference [14].
[b]Reference [13].
[c]Reference [12].
[d]Reference [44].

TABLE VI. The spectral distribution $dW_{B;A}/dy$ for the two-photon transition $2\,^1S_0 \to 1\,^1S_0$ in He-like ions, in units s^{-1}. The reduced photon energy $y = k^0_{f_1}/\Delta^{(1)}_{AB}$ is the fraction of the total transition energy transported by one of the two photons. The reduced FWHM are also given. Numbers in brackets denote powers of 10.

y	$Z = 28$	$Z = 36$	$Z = 41$	$Z = 50$	$Z = 64$	$Z = 70$	$Z = 80$	$Z = 90$	$Z = 92$
0.025	2.48[09]	1.09[10]	2.28[10]	6.78[10]	2.43[11]	3.79[11]	7.19[11]	1.24[12]	1.37[12]
0.050	5.16[09]	2.31[10]	4.92[10]	1.52[11]	5.77[11]	9.17[11]	1.78[12]	3.11[12]	3.44[12]
0.075	7.33[09]	3.32[10]	7.14[10]	2.24[11]	8.83[11]	1.43[12]	2.84[12]	5.05[12]	5.61[12]
0.100	9.10[09]	4.14[10]	8.97[10]	2.85[11]	1.15[12]	1.88[12]	3.80[12]	6.90[12]	7.68[12]
0.125	1.06[10]	4.82[10]	1.05[11]	3.36[11]	1.38[12]	2.27[12]	4.66[12]	8.58[12]	9.58[12]
0.150	1.18[10]	5.39[10]	1.17[11]	3.79[11]	1.57[12]	2.61[12]	5.42[12]	1.01[13]	1.13[13]
0.175	1.28[10]	5.86[10]	1.28[11]	4.16[11]	1.74[12]	2.90[12]	6.09[12]	1.15[13]	1.29[13]
0.200	1.36[10]	6.26[10]	1.37[11]	4.47[11]	1.89[12]	3.15[12]	6.67[12]	1.27[13]	1.42[13]
0.225	1.43[10]	6.60[10]	1.45[11]	4.73[11]	2.01[12]	3.37[12]	7.19[12]	1.37[13]	1.55[13]
0.250	1.49[10]	6.89[10]	1.51[11]	4.96[11]	2.12[12]	3.57[12]	7.64[12]	1.47[13]	1.66[13]
0.275	1.54[10]	7.13[10]	1.57[11]	5.15[11]	2.21[12]	3.73[12]	8.03[12]	1.55[13]	1.75[13]
0.300	1.58[10]	7.34[10]	1.61[11]	5.31[11]	2.29[12]	3.87[12]	8.37[12]	1.63[13]	1.84[13]
0.325	1.62[10]	7.51[10]	1.65[11]	5.45[11]	2.36[12]	4.00[12]	8.66[12]	1.69[13]	1.91[13]
0.350	1.65[10]	7.66[10]	1.68[11]	5.57[11]	2.42[12]	4.10[12]	8.90[12]	1.74[13]	1.97[13]
0.375	1.67[10]	7.77[10]	1.71[11]	5.66[11]	2.47[12]	4.18[12]	9.11[12]	1.79[13]	2.02[13]
0.400	1.69[10]	7.87[10]	1.73[11]	5.74[11]	2.50[12]	4.25[12]	9.27[12]	1.82[13]	2.07[13]
0.425	1.71[10]	7.94[10]	1.75[11]	5.79[11]	2.53[12]	4.30[12]	9.40[12]	1.85[13]	2.10[13]
0.450	1.72[10]	7.99[10]	1.76[11]	5.83[11]	2.55[12]	4.34[12]	9.49[12]	1.87[13]	2.12[13]
0.475	1.72[10]	8.02[10]	1.77[11]	5.86[11]	2.56[12]	4.36[12]	9.54[12]	1.88[13]	2.13[13]
0.500	1.73[10]	8.03[10]	1.77[11]	5.87[11]	2.57[12]	4.37[12]	9.56[12]	1.89[13]	2.14[13]
FWHM	0.814	0.809	0.804	0.793	0.771	0.761	0.743	0.722	0.718

confirms those of Ref. [10]. For the $2\,^3S_1$ state, the energy distribution function has two symmetric maxima in the first and second half of the unit segment. In the center point (equal energy sharing), the distribution function is zero for the decay channels with the photons with the same multipole numbers (e.g., for the 2E1 decay). This is a consequence of the Bose-Einstein statistics, which forbids us to construct a permutation symmetric two-photon state with total angular momentum $J_{\rm tot} = 1$. Therefore, near the center point the distribution function is defined by the E1M2 channel, as was noticed first in Ref. [43]. The value of y, where the first maximum is reached, is given in Table VII together with the corresponding values of the reduced FWHM. In contrast to the results reported in Ref. [10], we obtain a different energy distribution due to accounting for the higher multipole contributions.

IV. SUMMARY

In summary, we have presented a systematic quantum electrodynamic description for the first-order interelectronic-interaction corrections to the two-photon transition

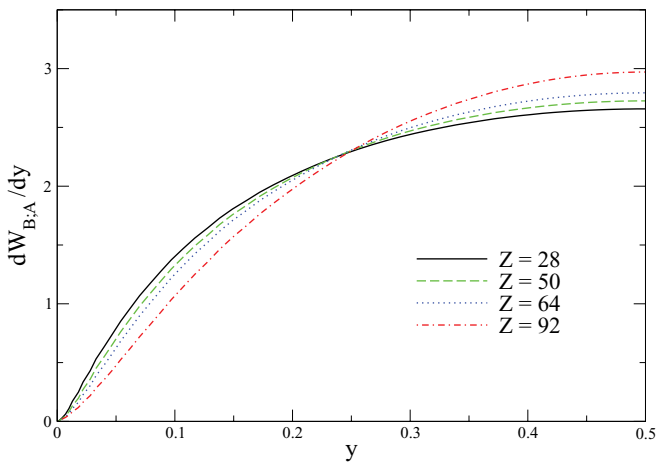

FIG. 6. (Color online) The $2\,^1S_0$ two-photon energy distribution functions $dW_{B;A}/dy$, normalized to the corresponding total decay rates, plotted as a function of the reduced energy y for He-like nickel, tin, europium, and uranium ions.

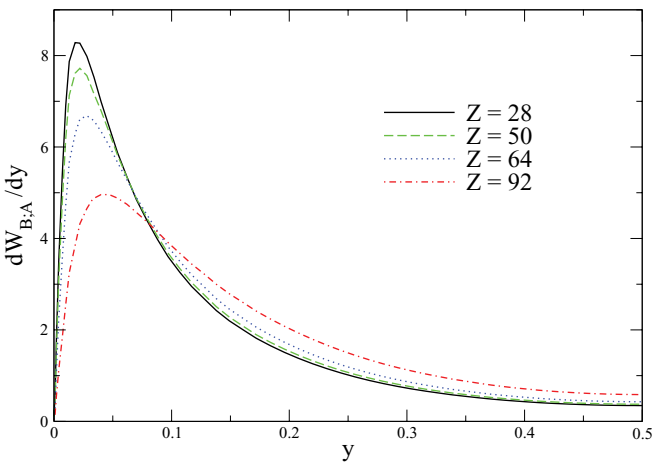

FIG. 7. (Color online) The $2\,^3S_1$ two-photon energy distribution functions $dW_{B;A}/dy$, normalized to the corresponding total decay rates, plotted as a function of the reduced energy y for He-like nickel, tin, europium, and uranium ions.

TABLE VII. The spectral distribution $dW_{B;A}/dy$ for the two-photon transition $2\,^3S_1 \to 1\,^1S_0$ in He-like ions, in units s^{-1}. The reduced photon energy $y = k^0_{f_1}/\Delta^{(1)}_{AB}$ is the fraction of the total transition energy transported by one of the two photons. The maximum point of the distribution y_{max} together with the reduced FWHM are also presented. Numbers in brackets denote powers of 10.

y	$Z = 28$	$Z = 36$	$Z = 41$	$Z = 50$	$Z = 64$	$Z = 70$	$Z = 80$	$Z = 90$	$Z = 92$
0.010	1.68[06]	2.27[07]	8.13[07]	5.12[08]	4.22[09]	8.62[09]	2.40[10]	5.71[10]	6.70[10]
0.015	1.94[06]	2.59[07]	9.32[07]	6.02[08]	5.21[09]	1.09[10]	3.13[10]	7.63[10]	8.99[10]
0.020	1.99[06]	2.64[07]	9.56[07]	6.30[08]	5.68[09]	1.21[10]	3.57[10]	8.92[10]	1.05[11]
0.025	1.95[06]	2.58[07]	9.37[07]	6.26[08]	5.85[09]	1.26[10]	3.83[10]	9.75[10]	1.16[11]
0.030	1.87[06]	2.46[07]	8.98[07]	6.08[08]	5.83[09]	1.28[10]	3.95[10]	1.03[11]	1.22[11]
0.035	1.78[06]	2.33[07]	8.52[07]	5.83[08]	5.72[09]	1.27[10]	3.99[10]	1.05[11]	1.26[11]
0.040	1.68[06]	2.19[07]	8.04[07]	5.55[08]	5.55[09]	1.24[10]	3.97[10]	1.06[11]	1.27[11]
0.045	1.58[06]	2.06[07]	7.57[07]	5.26[08]	5.35[09]	1.21[10]	3.91[10]	1.06[11]	1.28[11]
0.050	1.48[06]	1.94[07]	7.12[07]	4.98[08]	5.14[09]	1.17[10]	3.83[10]	1.05[11]	1.27[11]
0.075	1.10[06]	1.43[07]	5.30[07]	3.78[08]	4.10[09]	9.54[09]	3.27[10]	9.42[10]	1.14[11]
0.100	8.40[05]	1.09[07]	4.05[07]	2.93[08]	3.27[09]	7.72[09]	2.72[10]	8.08[10]	9.87[10]
0.125	6.58[05]	8.53[06]	3.17[07]	2.31[08]	2.63[09]	6.28[09]	2.26[10]	6.85[10]	8.41[10]
0.150	5.25[05]	6.81[06]	2.54[07]	1.86[08]	2.14[09]	5.15[09]	1.88[10]	5.80[10]	7.15[10]
0.175	4.26[05]	5.52[06]	2.06[07]	1.51[08]	1.77[09]	4.27[09]	1.58[10]	4.93[10]	6.08[10]
0.200	3.50[05]	4.54[06]	1.69[07]	1.25[08]	1.47[09]	3.57[09]	1.33[10]	4.20[10]	5.20[10]
0.225	2.91[05]	3.76[06]	1.41[07]	1.04[08]	1.23[09]	3.01[09]	1.13[10]	3.60[10]	4.46[10]
0.250	2.43[05]	3.15[06]	1.18[07]	8.75[07]	1.04[09]	2.55[09]	9.63[09]	3.09[10]	3.84[10]
0.275	2.06[05]	2.66[06]	9.97[06]	7.42[07]	8.88[08]	2.18[09]	8.28[09]	2.68[10]	3.33[10]
0.300	1.75[05]	2.27[06]	8.51[06]	6.34[07]	7.63[08]	1.88[09]	7.16[09]	2.33[10]	2.90[10]
0.325	1.51[05]	1.96[06]	7.33[06]	5.47[07]	6.61[08]	1.63[09]	6.25[09]	2.04[10]	2.54[10]
0.350	1.31[05]	1.70[06]	6.38[06]	4.77[07]	5.79[08]	1.43[09]	5.50[09]	1.80[10]	2.25[10]
0.375	1.15[05]	1.50[06]	5.63[06]	4.22[07]	5.14[08]	1.27[09]	4.90[09]	1.61[10]	2.01[10]
0.400	1.03[05]	1.34[06]	5.05[06]	3.79[07]	4.62[08]	1.15[09]	4.43[09]	1.46[10]	1.83[10]
0.425	9.42[04]	1.23[06]	4.61[06]	3.47[07]	4.24[08]	1.05[09]	4.08[09]	1.35[10]	1.69[10]
0.450	8.80[04]	1.15[06]	4.31[06]	3.24[07]	3.97[08]	9.87[08]	3.83[09]	1.27[10]	1.59[10]
0.475	8.43[04]	1.10[06]	4.14[06]	3.11[07]	3.82[08]	9.49[08]	3.68[09]	1.22[10]	1.53[10]
0.500	8.31[04]	1.08[06]	4.08[06]	3.07[07]	3.77[08]	9.36[08]	3.64[09]	1.21[10]	1.51[10]
y_{max}	0.020	0.019	0.020	0.019	0.024	0.030	0.035	0.041	0.043
FWHM	0.079	0.077	0.079	0.087	0.106	0.116	0.134	0.154	0.158

probabilities in He-like ions. A local screening potential has been included in the zeroth-order approximation in the framework of an extended Furry representation, and the corresponding expressions for the counterterms have been derived. Such a treatment of the electron-correlation effects allows us to control the gauge invariance of each term in the perturbation expansion and to estimate an uncertainty due to the truncation of this expansion. The total two-photon decay rates and the spectral distribution functions have been evaluated for the transitions $2\,^1S_0 \to 1\,^1S_0$ and $2\,^3S_1 \to 1\,^1S_0$ in the He-like ions with nuclear charges in the range $28 \leqslant Z \leqslant 92$. The results of the calculations performed have been compared with previous calculations and with experimental data. The present calculations of the two-photon decays of the $2\,^1S_0$ and $2\,^3S_1$ states in He-like ions can be utilized to study the parity nonconservation phenomena in He-like ions [21,45,46] as well as for investigations of the contributions of higher multipoles to the energy distribution.

ACKNOWLEDGMENTS

The authors owe thanks to D. A. Glazov and Th. Stöhlker for valuable comments and helpful discussions on this work. The work reported in this paper was supported by the Helmholtz Gemeinschaft and GSI (Project VH-NG-421), by the Deutsche Forschungsgemeinschaft (Grants No. VO 1707/1-1 and No. PL 254/7-1), by RFBR (Grant No. 10-02-00450), by the Russian Ministry of Education and Science (Grant No. P1334), and by a grant of the President of the Russian Federation (Grant No. MK-3215.2011.2). Computing resources were provided by the Zentrum für Informationsdienste und Hochleistungsrechnen (ZIH) at the TU Dresden.

[1] M. Göppert-Mayer, Ann. Phys. **9**, 273 (1931).
[2] G. W. F. Drake, Phys. Rev. A **34**, 2871 (1986).
[3] J. P. Santos, F. Parente, and P. Indelicato, Eur. Phys. J. D **3**, 43 (1998).
[4] A. Surzhykov, P. Koval, and S. Fritzsche, Phys. Rev. A **71**, 022509 (2005).
[5] L. N. Labzowsky, A. V. Shonin, and D. A. Solovyev, J. Phys. B **38**, 265 (2005).

[6] P. Amaro, J. P. Santos, F. Parente, A. Surzhykov, and P. Indelicato, Phys. Rev. A **79**, 062504 (2009).
[7] A. Dalgarno, Mon. Not. R. Astron. Soc. **131**, 311 (1966).
[8] O. Bely and P. Faucher, Astron. Astrophys. **1**, 37 (1969).
[9] G. W. F. Drake, G. A. Victor, and A. Dalgarno, Phys. Rev. **180**, 25 (1969).
[10] A. Derevianko and W. R. Johnson, Phys. Rev. A **56**, 1288 (1997).
[11] A. Surzhykov, A. Volotka, F. Fratini, J. P. Santos, P. Indelicato, G. Plunien, Th. Stöhlker, and S. Fritzsche, Phys. Rev. A **81**, 042510 (2010).
[12] R. Marrus, V. San Vicente, P. Charles, J. P. Briand, F. Bosch, D. Liesen, and I. Varga, Phys. Rev. Lett. **56**, 1683 (1986).
[13] R. W. Dunford, H. G. Berry, S. Cheng, E. P. Kanter, C. Kurtz, B. J. Zabransky, A. E. Livingston, and L. J. Curtis, Phys. Rev. A **48**, 1929 (1993).
[14] R. W. Dunford, H. G. Berry, D. A. Church, M. Hass, C. J. Liu, M. L. A. Raphaelian, B. J. Zabransky, L. J. Curtis, and A. E. Livingston, Phys. Rev. A **48**, 2729 (1993).
[15] P. H. Mokler, S. Reusch, A. Warczak, Z. Stachura, T. Kambara, A. Müller, R. Schuch, and M. Schulz, Phys. Rev. Lett. **65**, 3108 (1990).
[16] R. Ali *et al.*, Phys. Rev. A **55**, 994 (1997).
[17] H. W. Schäffer *et al.*, Phys. Lett. A **260**, 489 (1999).
[18] A. Kumar *et al.*, Eur. Phys. J. Special Topics **169**, 19 (2009).
[19] S. Trotsenko *et al.*, Phys. Rev. Lett. **104**, 033001 (2010).
[20] I. M. Savukov and W. R. Johnson, Phys. Rev. A **66**, 062507 (2002).
[21] V. M. Shabaev, A. V. Volotka, C. Kozhuharov, G. Plunien, and Th. Stöhlker, Phys. Rev. A **81**, 052102 (2010).
[22] A. Lapierre *et al.*, Phys. Rev. Lett. **95**, 183001 (2005).
[23] A. Lapierre *et al.*, Phys. Rev. A **73**, 052507 (2006).
[24] I. I. Tupitsyn, A. V. Volotka, D. A. Glazov, V. M. Shabaev, G. Plunien, J. R. Crespo López-Urrutia, A. Lapierre, and J. Ullrich, Phys. Rev. A **72**, 062503 (2005).
[25] A. V. Volotka, D. A. Glazov, G. Plunien, V. M. Shabaev, and I. I. Tupitsyn, Eur. Phys. J. D **38**, 293 (2006).
[26] A. V. Volotka, D. A. Glazov, G. Plunien, V. M. Shabaev, and I. I. Tupitsyn, Eur. Phys. J. D **48**, 167 (2008).
[27] P. Indelicato, V. M. Shabaev, and A. V. Volotka, Phys. Rev. A **69**, 062506 (2004).
[28] V. M. Shabaev, Izv. Vuz. Fiz. **33**, 43 (1990); Sov. Phys. J. **33**, 660 (1990).
[29] V. M. Shabaev, Teor. Mat. Fiz. **82**, 83 (1990); [Theor. Math. Phys. **82**, 57 (1990)].
[30] V. M. Shabaev, Phys. Rep. **356**, 119 (2002).
[31] O. Yu. Andreev, L. N. Labzowsky, and G. Plunien, Phys. Rev. A **79**, 032515 (2009).
[32] O. Yu. Andreev, L. N. Labzowsky, G. Plunien, and D. A. Solovyev, Phys. Rep. **455**, 135 (2008).
[33] V. B. Berestetsky, E. M. Lifshitz, and L. P. Pitaevsky, *Quantum Electrodynamics* (Pergamon, Oxford, 1982).
[34] C. Itzykson and J.-B. Zuber, *Quantum Field Theory* (McGraw-Hill, New York, 1980).
[35] L. Labzowsky, D. Solovyev, and G. Plunien, Phys. Rev. A **80**, 062514 (2009).
[36] L. N. Labzowsky and A. V. Shonin, Phys. Rev. A **69**, 012503 (2004).
[37] D. A. Glazov, A. V. Volotka, V. M. Shabaev, I. I. Tupitsyn, and G. Plunien, Phys. Lett. A **357**, 330 (2006).
[38] A. V. Volotka, D. A. Glazov, I. I. Tupitsyn, N. S. Oreshkina, G. Plunien, and V. M. Shabaev, Phys. Rev. A **78**, 062507 (2008).
[39] V. M. Shabaev, I. I. Tupitsyn, V. A. Yerokhin, G. Plunien, and G. Soff, Phys. Rev. Lett. **93**, 130405 (2004).
[40] I. Angeli, At. Data Nucl. Data Tables **87**, 185 (2004).
[41] Y. S. Kozhedub, O. V. Andreev, V. M. Shabaev, I. I. Tupitsyn, C. Brandau, C. Kozhuharov, G. Plunien, and T. Stöhlker, Phys. Rev. A **77**, 032501 (2008).
[42] A. N. Artemyev, V. M. Shabaev, V. A. Yerokhin, G. Plunien, and G. Soff, Phys. Rev. A **71**, 062104 (2005).
[43] R. W. Dunford, Phys. Rev. A **69**, 062502 (2004).
[44] A. Simionovici, B. B. Birkett, J. P. Briand, P. Charles, D. D. Dietrich, K. Finlayson, P. Indelicato, D. Liesen, and R. Marrus, Phys. Rev. A **48**, 1695 (1993).
[45] A. Schäfer, G. Soff, P. Indelicato, B. Müller, and W. Greiner, Phys. Rev. A **40**, 7362 (1989).
[46] L. N. Labzowsky, A. V. Nefiodov, G. Plunien, G. Soff, R. Marrus, and D. Liesen, Phys. Rev. A **63**, 054105 (2001).